THE ASTROPHYSICAL JOURNAL, 473:834–848, 1996 December 20


# THE DISTANCE TO TWO NEUTRAL HYDROGEN CLOUDS: THE HIGH-VELOCITY COMPLEX A AND THE LOW-LATITUDE INTERMEDIATE-VELOCITY CLOUD

BART WAKKER AND CHRIS HOWK
Department of Astronomy, University of Wisconsin, 475 North Charter Street, Madison, WI 53706;
wakker@astro.wisc.edu, howk@astro.wisc.edu

ULRICH SCHWARZ AND HUGO VAN WOERDEN
Kapteyn Astronomical Institute, Rijks Universiteit Groningen, Postbus 800, 9700 AV, Groningen, The Netherlands;
schwarz@astro.rug.nl, hugo@astro.rug.nl

TIMOTHY BEERS[1] AND RONALD WILHELM
Department of Physics and Astronomy, Michigan State University, East Lansing, MI 48824;
beers@pa.msu.edu, wilhelm@pa.msu.edu

PETER KALBERLA
Radioastronomisches Institut Universität Bonn, Auf dem Hügel 71, D-5300 Bonn 1, Germany;
kalberla@astro.um-bonn.de

AND

LAURA DANLY
Space Telescope Science Institute, 3700 San Martin Drive, Baltimore MD 21218; danly@stsci.edu
*Received 1996 May 8; accepted 1996 July 12*

## ABSTRACT

A lower limit to the distance of the high-velocity cloud (HVC) complex A of 4 kpc ($z > 3$ kpc) is derived. The HVC is detected toward the Seyfert galaxy Mrk 106 in Mg II $\lambda\lambda$2796, 2803 absorption spectra taken with *Hubble Space Telescope* (*HST*) proving that $Mg^+$ is present in the cloud. It is not detected in the Mg II spectra of two stars, PG 0859+593 (distance 4 kpc) and PG 0906+597 (distance 0.7 kpc). The distances to the stars are derived by matching Strömgren photometry and intermediate-resolution spectroscopy with model stellar atmospheres; they are estimated to be accurate to within 1 kpc. From a combination of Effelsberg data and Westerbork maps with 2′ or 3′ resolution, we show that the H I column density and thus the $Mg^+$ abundance in the direction of the two stars is sufficiently high for the nondetections to imply that the HVC is behind the stars. This distance limit can be used to eliminate several recent models for complex A that placed it nearby.

We also derive a distance bracket of $1.7 < d < 4$ kpc ($1.1 < z < 3$ kpc) for an intermediate-velocity cloud (IVC) at velocities of about $-50$ km s$^{-1}$. This IVC was named the Low-Latitude Intermediate-Velocity Arch by Kuntz & Danly and is seen between $\ell = 120°$–$160°$ and $b = 30°$–$45°$.

*Subject heading:* Galaxy: halo — ISM: clouds — radio lines: ISM — stars: distances

## 1. INTRODUCTION

Ever since their discovery in 1963 (Muller, Oort, & Raimond 1963), the high-velocity clouds (HVCs) have been enigmatic. HVCs are concentrations of neutral hydrogen moving with velocities inconsistent with a simple model of galactic rotation (for a review, see Wakker 1991a). In practice, one uses a lower limit of about 100 km s$^{-1}$ relative to the local standard of rest (LSR) to define the HVCs. Velocities up to $-450$ and $+300$ km s$^{-1}$ occur (Hulsbosch & Wakker 1988; Bajaja et al. 1985), and (depending on the definition one uses) between 10% and 37% of the sky is covered by such high-velocity gas (Wakker 1991b; Murphy, Lockman, & Savage 1995).

The sky and velocity distributions of the HVCs are now fairly well known (Wakker & van Woerden 1991). However, an understanding of their internal physics, their origin, and their role in galactic evolution requires a knowledge of their distances and composition. Over the years, many competing hypotheses for the origin of HVCs have been proposed. These models are primarily distinguished by the different distances at which the clouds are placed. Proposed explanations include local supernova remnants ($d \simeq 100$ pc), large-scale expanding motions in nearby spiral arms ($d \leq 1$ kpc), condensations in the local Galactic halo ($z \simeq 1$–5 kpc), structures in the Galactic warp ($d \simeq 5$–10 kpc), tidal disruption of the Magellanic Clouds ($d \simeq 20$–50 kpc), intergalactic gas ($d > 50$ kpc), or protogalaxies ($d \simeq 500$ kpc).

From survey data and individual observations, many indirect estimates of HVC distances have been made. Some of these assume that the HVCs are in the lower Galactic halo, at distances of the order of a few kiloparsecs (see, e.g., Oort & Hulsbosch 1978; Kaelble, de Boer, & Grewing 1985; Wakker 1991a). Much larger distances, on the order of 10–20 kpc, were suggested early on by Davies (1972a) and Verschuur (1973a). A distance of a few hundred parsecs was preferred by Meyerdierks (1991) and Verschuur (1993) for some HVC complexes. These arguments are all based on model assumptions, however, and they can provide only indirect information. A direct determination of distances is required to evaluate the proposed models.

The only known method to determine distances directly is to use interstellar absorption lines in the spectra of stars projected onto the HVC. This method and its many pitfalls are discussed in detail by Schwarz, Wakker, & van Woerden (1995). Here we give a short summary: an interstellar absorption component at the HVC's velocity pro-

[1] Visiting Astronomer, Kitt Peak National Observatory, which is operated by the Association of Universities for Research in Astronomy, under contract to the National Science Foundation.

vides an upper limit to the distance; a nondetection may yield a lower distance limit, but only if the expected absorption strength is well above the noise level. An estimate of the expected absorption strength requires a detection of the element or ion in the spectrum of an extragalactic object and an H I observation at the highest possible angular resolution toward both that extragalactic object and the probe in question. The H I map is necessary because of the presence of strong column density contrasts in some HVCs (up to a factor 5 on arcminute scales; see Wakker & Schwarz 1991).

The HVC that has been most intensively studied is complex A, an object 40° by 5° on the sky. Wakker & van Woerden (1991) give a description and references to earlier studies (see also § 2). To find suitable probes of complex A, we have used the data from the survey of Hulsbosch & Wakker (1988). By combining this survey with catalogs of suitable objects, we can identify the most promising candidate probes. Now that metallicities have actually been determined for a few HVCs (see Robertson et al. 1991; Lu, Savage, & Sembach 1994; Keenan et al. 1995; Wakker et al. 1996), it has become possible to make realistic estimates of the equivalent widths of HVC absorption, thereby allowing a better selection of probes.

To date, only one clear case exists of absorption by a HVC in a stellar probe: at $v_{\rm LSR} = -96$ km s$^{-1}$ in BD +38°2182, in the bridge between HVCs M II and M III. Combined with a nondetection toward HD 93521, this gives a distance constraint of $1.7 < d < 5.0$ kpc (Danly, Albert, & Kuntz 1993; Keenan et al. 1995). At visible wavelengths, Ca II H and K are expected to be the strongest interstellar absorption lines for high- and intermediate-velocity clouds. With *IUE* it has been possible to use ultraviolet resonance lines like those of Mg II, C II, and Si II, which are much stronger than the optical lines for a given column density of neutral gas. Nevertheless, no absorption by HVCs has been found for stars at distances up to 2 kpc (mostly toward complex C; Danly 1989; de Boer et al. 1994). These stars are at the limit of detectability with *IUE*. In this paper we report on *Hubble Space Telescope* (*HST*) absorption-line spectra of HVC complex A.

Goddard High-Resolution Spectrograph (GHRS) spectra of the Mg II doublet at 2800 Å have been taken of two stars and one extragalactic probe projected onto HVC complex A. In § 2 we justify our selection of probes. Section 3 discusses the classification of the stars and the derivation of their distance estimates. Section 4 presents the low- and high-resolution H I data necessary to derive the best possible value for the H I column density in the direction of the probes. In § 5 we describe the *HST* spectra. In § 6 we derive a distance limit for complex A, and in § 7 we discuss the implications for the HVC phenomenon.

## 2. PROBING COMPLEX A

### 2.1. *Previous Observations of Complex A*

HVC complex A was the first HVC discovered (Muller et al. 1963) and has been mapped extensively. It was originally named by Hulsbosch & Raimond (1966) and first mapped by Hulsbosch (1968), at 36′ and 10 km s$^{-1}$ resolution. Further mapping by Giovanelli, Verschuur, & Cram (1973), at 9′ and 1 km s$^{-1}$ resolution revealed the presence of several concentrations, which were named A I through A V; two further concentrations outside the scope of the data of Giovanelli et al. were later named A 0 and A VI (Wakker & van Woerden 1991). The brightest concentration is A IV, which was mapped at 12′ resolution by Davies, Buhl, & Jafalla (1976), while Hulsbosch (1978) mapped A 0 at 9′ resolution. The large-scale structure of complex A was revealed by the surveys of Giovanelli (1980) and Hulsbosch & Wakker (1988). These data also show substantial velocity differences between the concentrations, but there is no regular pattern to the velocity field. Figure 1 gives the distribution of H I brightness temperature from the latter survey for the part of the complex relevant to this paper.

Cram & Giovanelli (1976) used complex A to show the presence of two-component velocity structure in the profiles of HVCs. One component with a FWHM of about 23 km s$^{-1}$ was seen in all directions, while a second component with FWHM 7 km s$^{-1}$ was observed toward the cores. The presence of fine structure was attributed to fragmentation after shock compression, possibly following the passage of a supernova shock (Giovanelli & Haynes 1977). Early high-resolution mapping with interferometers by Schwarz, Sullivan, & Hulsbosch (1976) at 2′ resolution showed bright concentrations (25 K) in A 0, with densities of order $30/D_{\rm kpc}$ cm$^{-3}$ (here $D_{\rm kpc}$ is the distance in kpc). Schwarz & Oort (1981), Wakker (1991c), and Wakker & Schwarz (1991) mapped A I and A IV at 1′ and 2 or 1 km s$^{-1}$ resolution. Structure was found on scales down to the resolution of 1′. Gaussian fits to the profiles gave a typical FWHM of 5 km s$^{-1}$. The volume density was found to be between 50 and $200/D_{\rm kpc}$ cm$^{-3}$.

Wakker & Boulanger (1986) examined the *IRAS* 100 $\mu$m emission in the region around the A IV core and found no far-infrared emission associated with the HVC. They concluded that this implied either a dust abundance at least 3 times below the normal value for low-velocity gas or that the dust was too cool. The latter is possible if the cloud is more than 10 kpc above the Galactic plane.

Many characteristics that are considered general properties of HVCs have actually been derived from observations of complex A, as it is one of the brightest and largest HVCs. A determination of its distance may therefore set the scale of the whole HVC phenomenon, although for a full understanding, it will be necessary to derive a distance for each HVC separately.

Attempts at deriving the distance to HVC complex A have a long history. The first list of possible probes was published by Kepner (1968), who selected 17 B8–A5 stars between 8th and 13th mag at distances up to 1.5 kpc. Some of these were included in the samples of Songaila, Cowie, & Weaver (1988) and Lilienthal, Meyerdierks, & de Boer (1990), who derived a firm lower distance limit of 500 pc for complex A based on main-sequence A stars. Songaila et al. (1988) further claimed a tentative detection of absorption due to complex A in the spectrum of the A0 V star SA 12 391 (distance about 1.7 kpc), but Lilienthal et al. (1990) conclusively showed this line to be stellar. The reinterpretation of the Songaila et al. (1988) spectrum therefore sets a lower distance limit of 1.7 kpc for HVC complex A.

The star PG 0905+626 has an estimated distance between 3 and 4.5 kpc and at first appeared a very useful probe. M. Pettini (1986, private communication) reported a nondetection of the Ca II K line toward this star. However, a subsequent Westerbork map (Wakker & Schwarz 1991) illustrated the problems associated with H I fine structure. They showed that this star falls within an area of depressed

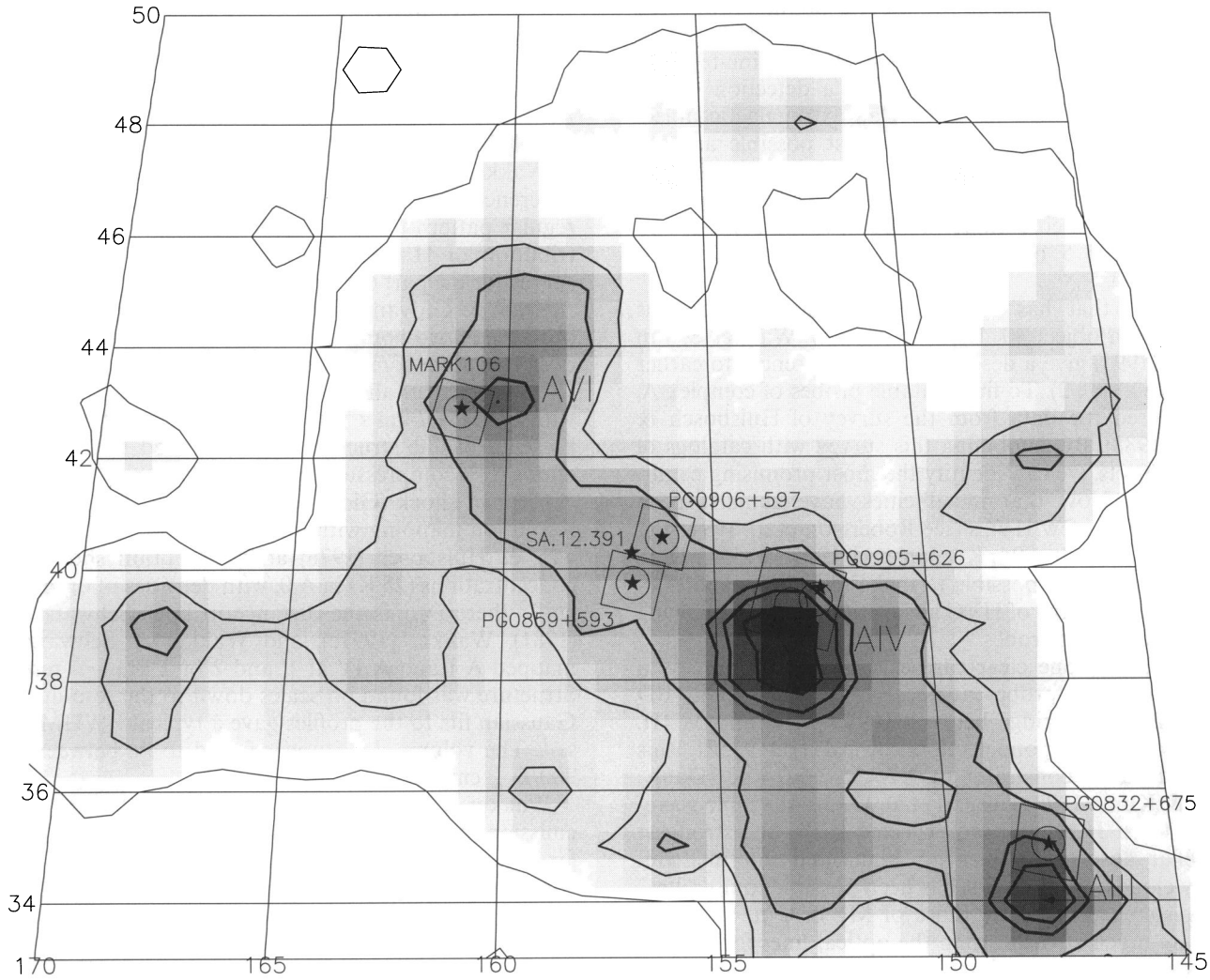


FIG. 1.—Combined gray-scale and contour map of the brightness temperature distribution of HVC complex A, based on the survey data of Hulsbosch & Wakker (1988). Contour levels are at 0.04, 0.30, 0.60, 1.5, 2.0 and 3.0 K. The main concentrations A III, A IV and A VI are indicated (A V does not show up well in this survey). The star symbols indicate the positions of the three probes discussed in this paper, as well as three probes from previous papers (see §§ 2.2 and 6). Around the five probes observed at Westerbork, the diameter of the Westerbork primary beam (FWHM 36′) is indicated. Also, the boundaries of the Westerbork maps are shown. For the three probes discussed in this paper, these are the same boundaries as shown in Fig. 3. For the A IV field, it is the boundary of the box in Fig. 1*a* of Wakker & Schwarz (1991), and for PG 0832+675, it is the box of Fig. 7*c* in Schwarz et al. (1995). The orientation of these boxes is such that the highest declination is to the left-hand side, and the highest right ascension is to the bottom side.

H I emission. The nondetection of absorption is therefore not significant.

Brown et al. (1989) and Schwarz et al. (1995) reported a nondetection of Ca II H and K absorption for PG 0832+675 (with velocity resolutions of 40 and 26 km $s^{-1}$, respectively). Schwarz et al. (1995) derived that $Ca^+/H$ toward this star is $< 12 \times 10^{-9}$ (3 $\sigma$). By comparing this to the value of $17 \pm 6 \times 10^{-9}$ found toward the Seyfert galaxy Mrk 106, they tentatively concluded that the HVC is behind the star. The detection toward Mrk 106 was recently confirmed at higher signal-to-noise ratio (S/N) (van Woerden et al. 1996). If PG 0832+675 were an sdO star as classified by Green, Schmidt, & Liebert (1986), its distance would be of the order of 2.5 kpc (Schwarz et al. 1995 prefer 1.6 kpc, using the faint end of the range of absolute magnitudes). Brown et al. studied PG 0832+675 in more detail and concluded that it is a Population I B star at a distance of 31 kpc ($z = 18$ kpc). However, there are now indications that the distance is only a few kiloparsecs (Hambly et al. 1996). For a discussion of the phenomenon of high-$z$ stars that mimic early-type main-sequence stars, see Sasselov (1993).

We will now discuss how we arrived at the selection of the probes discussed in this paper.

### 2.2. *Stellar Probes*

The process of selecting probes of HVCs is described in detail by Schwarz et al. (1995). In principle, main-sequence A stars are useful. However, at high Galactic latitudes, they are too faint when at large distances. Blue horizontal branch (hereafter BHB) stars and subdwarfs are the preferred kind of probes, as they have reasonably well-determined absolute magnitudes, are comparatively numerous at high Galactic latitudes and can be seen to distances of several kiloparsecs at an apparent magnitude of 16 (the limit of current instrumentation at the required velocity resolution of 20 km $s^{-1}$ or less). To find probes of HVC complex A, the most important survey for our purposes is the Palomar-Green (PG) list (Green et al. 1986), in which 14 candidate probes can be found. Newer surveys of

faint blue objects also exist (mainly the HK survey of Beers, Preston, & Schectman 1988, and Beers et al. 1996). Few of these surveys overlap with complex A, however, and for most probe candidates, only rough information on the spectral type and distance is available. Using the same techniques as employed in these newer surveys, it will be possible in the future to expand the sample of candidate probes for complex A and other HVCs.

To select the best probes from the PG list projected onto complex A, we first estimated their distances. For subdwarfs, absolute magnitudes of $M_V$ (sdO) = 1.8–3.2, and $M_V$ (sdB) = 2.9–3.9 were assumed. These values are based on the determinations of $T_{\rm eff}$ and log $g$ for stars in the PG sample given by Moehler, Heber, & de Boer (1990a), Moehler et al. (1990b), Dreizler et al. (1990), Theissen et al. (1993), and Beers et al. (1992). For BHB stars, the polynomial fit to the shape of the horizontal branch from globular cluster color-magnitude diagrams obtained by Preston, Schectman, & Beers (1991) was used, which allows one to estimate the absolute magnitude given a $B-V$ color. The relation is valid over the color range $B-V = -0.2$ to $+0.2$, corresponding to $M_V = 2.9$–$0.6$. If no color is given, we assumed a most likely color of $B-V = 0.05$, or $M_V = 0.85$. For a 15th mag star this means that the distance will be estimated as 6.8 kpc but could range between 2.6 and 7.6 kpc.

Using the assumptions detailed above, the most distant probe of complex A in the PG sample is the BHB star PG 0859+593. Using the method outlined above, it appeared to be at a distance of ~9 kpc, but we will show that it is more likely to be at 4 kpc. The other 13 stars are subdwarfs at distances between a few hundred parsecs and 4 kpc. For our *HST* project, we selected the two most distant probes for which reasonably strong absorption can be expected: PG 0859+593 and PG 0906+597.

### 2.3. *Extragalactic Probes*

To determine the significance of a nondetection in the spectrum of a stellar probe, a detection of HVC absorption toward an extragalactic probe is required. Quasars and Seyfert galaxies are the most suitable for this, although Seyfert galaxies are usable only if enough flux comes from the core. To find extragalactic probes, we have correlated the catalog of Véron-Cetty & Véron (1995) with the data from Hulsbosch & Wakker (1988). This yielded nine Seyfert galaxies and three QSOs projected onto complex A. The four brightest Seyfert galaxies (all having an NGC number) are extended, so their cores are not sharp enough to function as good background sources. Two of the QSOs and four of the Seyfert galaxies are projected onto a very low column density part of the HVC. This leaves two possible probes, of which the one more likely to yield detectable interstellar absorption (based on the expected equivalent width of the absorption) is the Seyfert galaxy Markarian 106.

## 3. STELLAR CLASSIFICATION

To derive reliable distances for our two probe stars, Strömgren photometry was obtained at the KPNO 0.9 m telescope, using the CCDPHOT system. Both stars are rather faint for observations with this setup, and portions of the nights were not absolutely photometric; however, according to the observer (A. Sarajedini), there is no clear reason for rejecting the data (i.e., standard stars observed close to the PG stars transformed to the standard system well). Data reductions were carried out by B. Anthony-Twarog, using procedures similar to those outlined in Twarog & Anthony-Twarog (1995). Since the PG stars were not part of the main program effort, the selection of standard stars was less than optimal, and the bluest standard used had a color $b-y = 0.2$. For all of the above reasons, we have doubled the formal errors given by the data reduction process (see Table 1).

Interstellar reddening $[E(B-V)]$ in the direction toward these stars was determined from the Burstein & Heiles (1982) maps. This reddening was transformed to the Strömgren system using the standard relation $E(b-y) = 0.74\ E(B-V)$ (Crawford 1975). Interstellar absorption was calculated by adopting $A_V = 3.2\ E(B-V)$. The $m_1$ and $c_1$ indices were dereddened using the relations $m_0 = m_1 + 0.3\ E(b-y)$ and $c_0 = c_1 - 0.2\ E(b-y)$ (Crawford 1975). Green (1980) also obtained Strömgren photometry for the star PG 0906+597. His observations ($V = 15.37 \pm 0.05$, $b-y = -0.18 \pm 0.02$, $m_1 = 0.08$, $c_1 = -0.21$) are in excellent agreement with our newly obtained values, within the quoted errors.

Medium-resolution (2 Å, 3 pixels FWHM) spectroscopy over the wavelength interval 3700–5000 Å was obtained for both stars using the KPNO 2.1 m telescope and the GoldCam spectrograph with a 600 line mm$^{-1}$ grating, imaging onto the F3KC CCD detector through a 2″ slit. The spectra are shown in Figure 2. In order to calibrate these spectra, observations before and after each program object were obtained of the flux standard PG 0934+554 (Massey et al. 1988). Standard IRAF procedures were followed to bias-subtract, flat-field correct, extract, wavelength-calibrate, and flux-calibrate the data.

Estimates of surface temperatures were obtained for each star by comparing the observed Strömgren color indices to the Kurucz color calibrations calculated from Atlas 9 model atmospheres (R. L. Kurucz 1992, private communication). Colors from the solar metallicity models were employed since both stars are hot enough that metallic-line blanketing effects should not be important. The best simultaneous match to the $(b-y)_0$, $c_0$, and $m_0$ indices was found for each star.

The spectrum of PG 0859+593 exhibits the broad and deep Balmer lines and neutral He absorption of a medium-to-late B-type star. The match in color indicates a temperature of $T_{\rm eff} = 12{,}500$ K and surface gravity log $g = 3.5$. A comparison of the line profile of H$\delta$ with synthetic spectra, following techniques discussed in detail by Wilhelm (1995), suggests a similar temperature, but a surface gravity closer to log $g = 4.0$. Unfortunately, log $g$ cannot be used as a luminosity class indicator because high-luminosity main-sequence stars and the lower luminosity horizontal-branch stars have similar surface gravities at this temperature. Under the conservative assumption that PG 0859+593 is a horizontal-branch star, the distance was estimated using the $M_V$ versus $B-V$ calibration for horizontal-branch stars given by Preston et al. (1991), after transforming the observed $(b-y)_0$ to $(B-V)_0$. This yields $M_V = 1.87$, corresponding to a distance of $4 \pm 1$ kpc from the Sun ($2.5 \pm 0.6$ kpc above the disk). This distance is much less than originally estimated because the star is as much as 0.15 mag bluer than our original assumption.

In the case of PG 0906+597, the observed colors are too blue to match the highest temperature ($T_{\rm eff} = 50{,}000$ K)

TABLE 1

OBSERVATIONAL PARAMETERS

| PARAMETER | OBJECT | | |
|---|---|---|---|
| | Mrk 106 | PG 0859+593 | PG 0906+597 |
| R.A. (2000) | 09 19 55 | 09 03 03 | 09 10 21 |
| Decl. (2000) | +55 21 37 | +59 11 18 | +59 30 34 |
| $l$ | 161.14 | 156.94 | 156.22 |
| $b$ | 42.88 | 39.74 | 40.56 |
| **Stellar Classification** | | | |
| Photometry observing date | ... | 1995 Nov 16/17 | 17/18 Nov 95 |
| Spectroscopy observing date | ... | 1995 Oct 29/30 | 15/16 May 96 |
| $V$ | 16.15 | $15.00 \pm 0.04$ | $15.43 \pm 0.18$ |
| $B-V$ or $b-y$ | −0.94 | $-0.02 \pm 0.06$ | $-0.13 \pm 0.16$ |
| $U-B$ | 0.39 | ... | ... |
| $m_1$ | ... | $0.08 \pm 0.08$ | $0.04 \pm 0.06$ |
| $c_1$ | ... | $0.67 \pm 0.04$ | $-0.21 \pm 0.07$ |
| $E(b-y)$ | | 0.03 | 0.03 |
| $V_0$ | ... | $14.89 \pm 0.04$ | $15.23 \pm 0.18$ |
| $(b-y)_0$ | | $-0.05 \pm 0.06$ | $-0.16 \pm 0.16$ |
| $m_0$ | ... | $0.09 \pm 0.08$ | $0.05 \pm 0.06$ |
| $c_0$ | ... | $0.66 \pm 0.04$ | $-0.22 \pm 0.07$ |
| $T_{\rm eff}$ (K) | ... | 12,500 | 75,000 |
| log $g$ | ... | 3.5–4.0 | ~6.8 |
| Type | Sey | BHB | sdO |
| Distance (kpc) | inf | $4 \pm 1$ | $0.7 \pm 0.2$ |
| **Dwingeloo Survey Data**[a] | | | |
| $v_{\rm LSR}$(Dw) (km s$^{-1}$) | −157 | −160 | −153 |
| $T_B$ (Dw) (K) | 0.75 | 0.56 | 0.56 |
| **Effelsberg Observations** | | | |
| Observing date | 1988 Feb 4 | 1995 Jan 12 | 1995 Jan 12 |
| Integration time (minutes) | 15 | 9 | 6 |
| Beam (arcmin) | 9 | 9 | 9 |
| Velocity resolution (km s$^{-1}$) | 1.288 | 1.288 | 1.288 |
| rms (K) | 0.02 | 0.09 | 0.09 |
| **Westerbork Observations**[b] | | | |
| Observation dates | 1988 May 11 (36 m) | 1993 Sep 23 (54 m) | 1993 Aug 27 (36 m) |
| | 1993 Sep 17 (54 m) | ... | 1994 Mar 7 (72 m) |
| | 1988 Mar 23 (72 m) | ... | 1993 Nov 30 (72 m) |
| | 1993 Dec 9 (90 m) | ... | ... |
| Grating ring radius (arcmin) | 40 | 10 | 20 |
| Velocity resolution (km s$^{-1}$) | 1.03 | 2.07 | 2.07 |
| Velocity range (km s$^{-1}$) | 36,72: −221 to +41 | −250 to +11 | −250 to +11 |
| | 54,90: −250 to +11 | ... | ... |
| Beam[c] (arcmin) | 3.44 × 3.13 | 3.62 × 3.60 | 1.78 × 1.77 |
| K/(mJy beam$^{-1}$) | 0.0158 | 0.0129 | 0.053 |
| rms[d] (mJy beam$^{-1}$) | 8.7 | 13.2 | 5.8 |
| rms[d] (K) | 0.14 | 0.17 | 0.30 |
| ***HST* Observations** | | | |
| Observing date | 1995 Mar 13 | 1993 Nov 7 | 1993 Nov 7 |
| Aperture | LSA | LSA | LSA |
| Grating | G270M | G270M | G270M |
| Wavelength range (Å) | 2777–2822 | 2777–2822 | 2777–2822 |
| Number of subexposures | 68 | 32 | 28 |
| Integration time (s) | 6963.2 | 3278.8 | 2867.2 |
| Velocity resolution (km s$^{-1}$) | 10.6 | 10.6[e] | 10.6[e] |
| Continuum counts @ Mg II | 30 | 28 | 78 |
| S/N continuum @ Mg II | 5.0 | 4.5 | 8.9 |

NOTE.—Units for night ascension are hours, minutes, and seconds, and units for declination are degrees, arcminutes, and arcseconds.

[a] Interpolation from the Hulsbosch & Wakker 1988 survey.

[b] For WSRT observing dates, the shortest baseline in meters is also given.

[c] The WSRT beam is the beam of the final map, shown in Fig. 3.

[d] Noise in WSRT map at given resolution.

[e] The spectral spread function has a core of ~10 km s$^{-1}$ FWHM and broad wings out to ~ ±40 km s$^{-1}$.

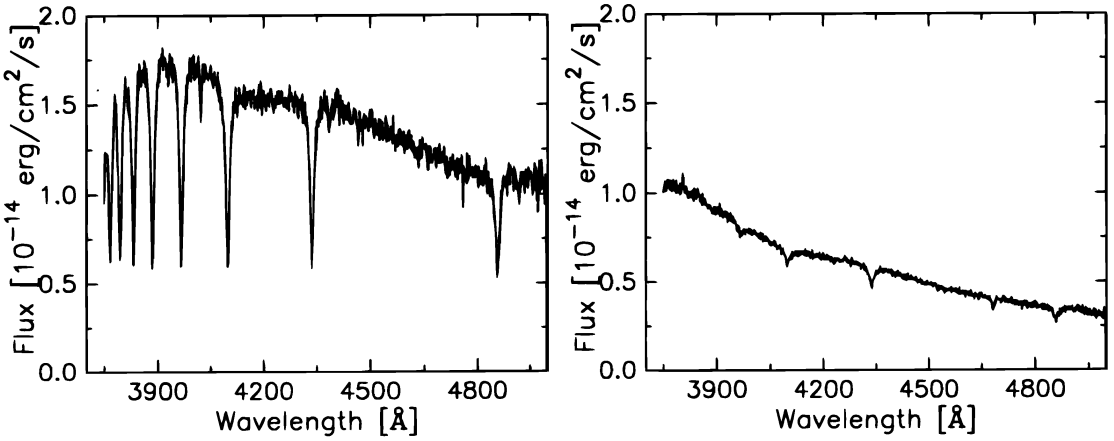


FIG. 2.—Intermediate-resolution spectra for PG 0859+593 (*left*) and PG 0906+597 (*right*) showing that PG 0859+593 is a horizontal-branch star (compare Fig. 6 of Beers et al. 1992). PG 0906+597 has a spectrum indicating a very hot sdO or hot white dwarf star.

Kurucz model, which suggests that this star might be an sdO star with temperature in excess of 50,000 K. However, its spectrum exhibits broad and shallow Balmer lines, and a weak He II $\lambda$4686 feature, rather different than the hot sdO stars of similar temperatures described in Thjell et al. (1994) or Drilling & Beers (1995). A preliminary model atmosphere analysis of this spectrum (U. Heber, private communication) suggests that PG 0906+597 may be a member of the small class of stars identified as DAO, some of which appear to be the central stars of newly formed planetary nebulae, while others are identified as spectroscopic binaries (see Heber, Dreizler, & Hagen 1996).

Heber's spectral analysis yields $T_{\rm eff} = 74{,}000 \pm 3000$ K, $\log g = 6.8 \pm 0.09$ (note that these errors are *internal* estimates obtained from the spectral fit—external estimates would certainly be higher). Such a surface gravity is higher than that generally associated with sdO stars and is more consistent with the low end of surface gravities for hot white dwarfs. Adopting a mass of 0.5 $M_\odot$, Heber suggests an absolute magnitude on the order of $M_V = 6.0$. The resulting distance estimate, 700 pc, is substantially lower than that which would be obtained if the sdO classification were adopted (1–2 kpc). If the mass of PG 0906+597 is as low as 0.3 $M_\odot$, the distance estimate drops to $\sim$500 pc. Clearly, more detailed spectroscopic information would be desirable for PG 0906+597. In addition, it would be useful to search for any evidence of binarity or nascent nebulosity associated with this object.

## 4. H I DATA

### 4.1. *Summary*

In order to derive the best estimate of the H I column density toward our three probes, we obtained H I observations with both the Effelsberg telescope (9′ beam) and with the Westerbork Synthesis Radio Telescope (2′ or 3′ beam). The highest possible resolution is required, as previous observations of HVCs have shown significant fine structure (Schwarz & Oort 1981; Wakker & Schwarz 1991). In practice, we can reach a resolution between 1′ and 3′ with the Westerbork synthesis telescope and still have detectable signal. To estimate the total column density in a particular direction, one has to keep in mind that the interferometer data show only the H I fine structure. Extended emission is filtered out by the interferometric process, because the zero and short spacings are not observed. The Effelsberg observations provide some information about the missing spacings. A full discussion of the need for high-resolution H I observations and of several other considerations is given in § 4 of Schwarz et al. (1995).

Below, we will describe in detail how we derived the best estimates for the H I column density in the direction of the probes. The final results are given in Table 2. These estimates are the sum of three terms. The first term is the brightness temperature measured with the 9′ Effelsberg beam. From this is subtracted the contribution of smaller scale structure found by smoothing the Westerbork map from 2′ or 3′ to 9′ resolution. Then the brightness temperature observed in the Westerbork maps is added. The errors in the final estimate are found from the measurement errors in the Effelsberg spectrum and systematic errors in the correction terms due to small-scale structure that is fainter than the noise level of the high-resolution maps. For the HVC components toward our three probes, the corrections turn out to be small, while for the IVC component toward PG 0906+597, the correction is more than a factor of 2.

The percentage of the flux that is in the small-scale structure ($<10'$) relative to that in smoother structures ($>20'$) is only about 10%. These numbers are rough guidelines. A more precise study is outside the scope of this paper. However, they can be contrasted with earlier results on other HVC cores where about 25%–50% of the structure is on small scales (Wakker & Schwarz 1991). Apparently, there is less fine structure in the envelopes than in the cores of HVCs. Since we do not have single-dish data with a 36′ beam available for the IVCs, we are unable to derive such percentages for them.

### 4.2. *Effelsberg Observations*

The Effelsberg observations were done for us by P. Kalberla of the University of Bonn. The relevant parameters of the observations are included in Table 1. The spectra were calibrated using the standard field S7, according to the method described by Kalberla, Mebold, & Reif (1982). They have also been corrected for stray radiation (Kalberla, Mebold, & Reich 1980). The final spectra are displayed in Figure 4 in the panel labeled (Eff).

Gaussian fits were made to each of the components discernible in the Effelsberg spectra. These fits were done in a

TABLE 2

RESULTS

| Object | $v_{LSR}$ (km s$^{-1}$) | FWHM (km s$^{-1}$) | $T_{B,peak}$ (K) | $N$ (H I, Eff) ($10^{18}$ cm$^{-2}$) | $N$ (H I, final) ($10^{18}$ cm$^{-2}$) | $W$ (2796)[a] (mÅ) | $W$ (2803)[a] (mÅ) | $N$ (Mg II)[b] ($10^{13}$ cm$^{-2}$) | $A$ (Mg II) ($10^{-8}$) |
|---|---|---|---|---|---|---|---|---|---|
| Mrk 106 ..... | $-157.2 \pm 0.1$ | $29.5 \pm 0.3$ | $0.67 \pm 0.01$ | $38.4 \pm 0.5$ | $38^{+2.4}_{-2.9}$ | $526 \pm 22$ | $490 \pm 26$ | $\geqslant 5$ | $\geqslant 130$ |
| | $-38.6 \pm 0.3$ | $32.9 \pm 0.9$ | $0.41 \pm 0.01$ | $26.2 \pm 0.6$ | $26^{+2.5}_{-3.2}$ | $319 \pm 14$ | $321 \pm 14$ | $\geqslant 4$ | $\geqslant 150$ |
| | $-3.7 \pm 0.1$ | $15.3 \pm 0.1$ | $6.05 \pm 0.01$ | $180.0 \pm 0.3$ | $213^{+2.2}_{-1.5}$ | $355 \pm 15$ | $359 \pm 16$ | $\geqslant 3$ | $\geqslant 14$ |
| | $-6.8 \pm 0.1$ | $2.7 \pm 0.1$ | $6.34 \pm 0.02$ | $33.2 \pm 0.1$ | ... | ... | ... | ... | ... |
| PG 0859+593..... | $-165.9 \pm 0.5$ | $23.9 \pm 1.1$ | $0.73 \pm 0.03$ | $33.8 \pm 1.4$ | $34^{+3.7}_{-3.3}$ | $0 \pm 32$ | $0 \pm 32$ | $<0.23$ | $< 6.8$ |
| | $-51.6 \pm 0.2$ | $19.0 \pm 0.4$ | $1.96 \pm 0.03$ | $72.2 \pm 1.1$ | $53^{+3.4}_{-2.6}$ | $400 \pm 12$ | $372 \pm 14$ | $\geqslant 4$ | $\geqslant 75$ |
| | $-0.3 \pm 0.1$ | $11.5 \pm 0.1$ | $11.69 \pm 0.04$ | $260.8 \pm 0.9$ | $250^{+3.2}_{-1.8}$ | $478 \pm 17$ | $429 \pm 19$ | $\geqslant 4$ | $\geqslant 16$ |
| PG 0906+597..... | $-152.6 \pm 0.4$ | $23.5 \pm 1.0$ | $0.80 \pm 0.03$ | $36.5 \pm 1.4$ | $29^{+5.4}_{-3.2}$ | $0 \pm 16$ | $0 \pm 16$ | $<0.12$ | $< 4.1$ |
| | $-53.5 \pm 0.1$ | $6.0 \pm 0.1$ | $3.86 \pm 0.07$ | $44.9 \pm 0.8$ | $110^{+6.1}_{-4.2}$ | $0 \pm 16$ | $0 \pm 16$ | $<0.12$ | $< 1.1$ |
| | $-48.2 \pm 0.3$ | $27.5 \pm 0.7$ | $1.59 \pm 0.04$ | $84.8 \pm 2.1$ | ... | ... | ... | ... | ... |
| | $-0.7 \pm 0.1$ | $13.3 \pm 0.1$ | $10.71 \pm 0.07$ | $276.3 \pm 1.8$ | $341^{+5.8}_{-2.8}$ | $364 \pm 15$ | $352 \pm 14$ | $\geqslant 2.5$ | $\geqslant 7$ |
| | $-2.6 \pm 0.1$ | $2.8 \pm 0.1$ | $4.58 \pm 0.10$ | $24.9 \pm 0.5$ | ... | ... | ... | ... | ... |

NOTE.—For the three cases in which a broad and a narrow component are seen in the H I spectrum, the two have been combined for the derivation of abundance limits, because they cannot be separated in the Mg II spectra.

[a] Errors are 1 $\sigma$ fitting errors.

[b] Mg II column density lower and upper limits derived from the $\lambda$2803 line; upper limits are 3 $\sigma$ limits.

piecewise fashion, i.e., three velocity ranges were separately fitted. A single three-, four-, or five-component fit to the full spectrum gives the same results for most components, but in a few cases such a fit diverged. We preferred the result of the piecewise fits, which usually yielded a single Gaussian component but sometimes required a combination of a broad (FWHM $\sim$ 15 km s$^{-1}$) and a narrow (FWHM $\sim$ 3 km s$^{-1}$) component. For PG 0859+593, the intermediate-velocity component appears non-Gaussian, but the fitting algorithm did not converge on a two-component fit, and a single Gaussian was used as an approximation. The final results are given in Table 2, with peak brightness temperatures of 0.67, 0.73, and 0.80 K for the HVC components toward Mrk 106, PG 0859+593, and PG 0906+597, respectively.

### 4.3. *Westerbork Observations*

The descriptions of the Westerbork observations of fields around our three probes are included in Table 1. For PG 0906+597 and Mrk 106, observing and reduction procedures are similar to those described by Wakker (1991c). In the case of Mrk 106, an earlier version of this map was presented by Schwarz et al. (1995), based only on the observations with shortest baselines of 36 and 72 m. Of several observations of the PG 0859+593 field, only one is usable. It has a shortest baseline of 54 m. The other observations suffer from interference and other technical difficulties. The reduction for this field is therefore more difficult. However, a single Westerbork observation with 54 m as the shortest baseline has the special feature that the beam is flat within the radius of the first grating ring. So, a usable map could still be extracted.

For all fields, the original data had a longest baseline corresponding to a resolution of 0.5. However, the signal-to-noise ratio is too low at those scales, and the longer baselines were not included in the mapping, so that the final maps have resolutions of 2′–3′ (see Table 1). Only faint continuum sources are present in these fields, none bright enough to allow the detection of H I absorption due to the HVC. The continuum was subtracted, and then the maps were cleaned, using the Multi-Resolution Clean algorithm (Wakker & Schwarz 1988). Delimiting boxes were chosen around all apparent emission features. The cleaned maps were then checked for remaining sidelobes, and the process was repeated if necessary. Usually this procedure works well. However, for the low-velocity emission in the Mrk 106 field, not all sidelobes could be fully removed. Also, in the PG 0859+593 field, it was not always possible to separate sidelobes from real signal because of the small (10′) radius of the inner grating ring. For these problematic cases, the structures visible in the final maps may not always be reliable.

To construct total column density maps, the cleaned maps were first smoothed to a resolution of 5′. Areas in the smoothed map where the signal is above 2 $\sigma$ then define a mask. This mask is applied to the channels at the original resolution to select the areas containing signal. The signal was then summed and converted to column densities, using the relations $N(\mathrm{H\ I}) = 1.823 \times 10^{18} \int T_B(v)dv$ and $T_B(\mathrm{K}) = 594\ S\ [\mathrm{mJy\ beam}^{-1}]/(\Delta\alpha\Delta\delta)\ [\mathrm{arcsec}^2]$, where $S$ is the flux, and $\Delta\alpha$ and $\Delta\delta$ are the spatial resolutions (FWHM) in right ascension and declination, respectively. The maps were corrected for the primary beam attenuation by dividing them by a Gaussian with an FWHM of 36′, allowing a maximum correction of a factor 8, corresponding to a field of view with a diameter of 1°. Figure 3 presents the final column density maps of the fine structure for the three fields. In these maps, the position of the optical probe is also indicated, as are the FWHM of the Effelsberg beam and the FWHM of the Westerbork primary beam.

#### 4.3.1. *Final Column Densities toward the Probes*

To derive the hydrogen column density in the direction of our probes, we have to combine the Effelsberg and Westerbork data. The main problem is the uncertainty in the Westerbork results due to the missing short spacings. This information can be recovered only by using an interferometer with smaller dishes, by mapping the whole field with a single-dish telescope with a diameter larger than the 25 m dishes used in Westerbork, or by using an interferometer in a mosaicking mode. Without this information, we can still make a fair estimate of the column density in the direction of the probes in the following manner. First, find the brightness temperature in the direction of the probe as measured with the Effelsberg beam [Fig. 4, panel (Eff)]. Second, smooth the Westerbork map to the resolution of the Effelsberg beam (9′) and find the brightness temperature in the direction of the probe [Fig. 4, panel (WSRT/Eff)]. The dif-

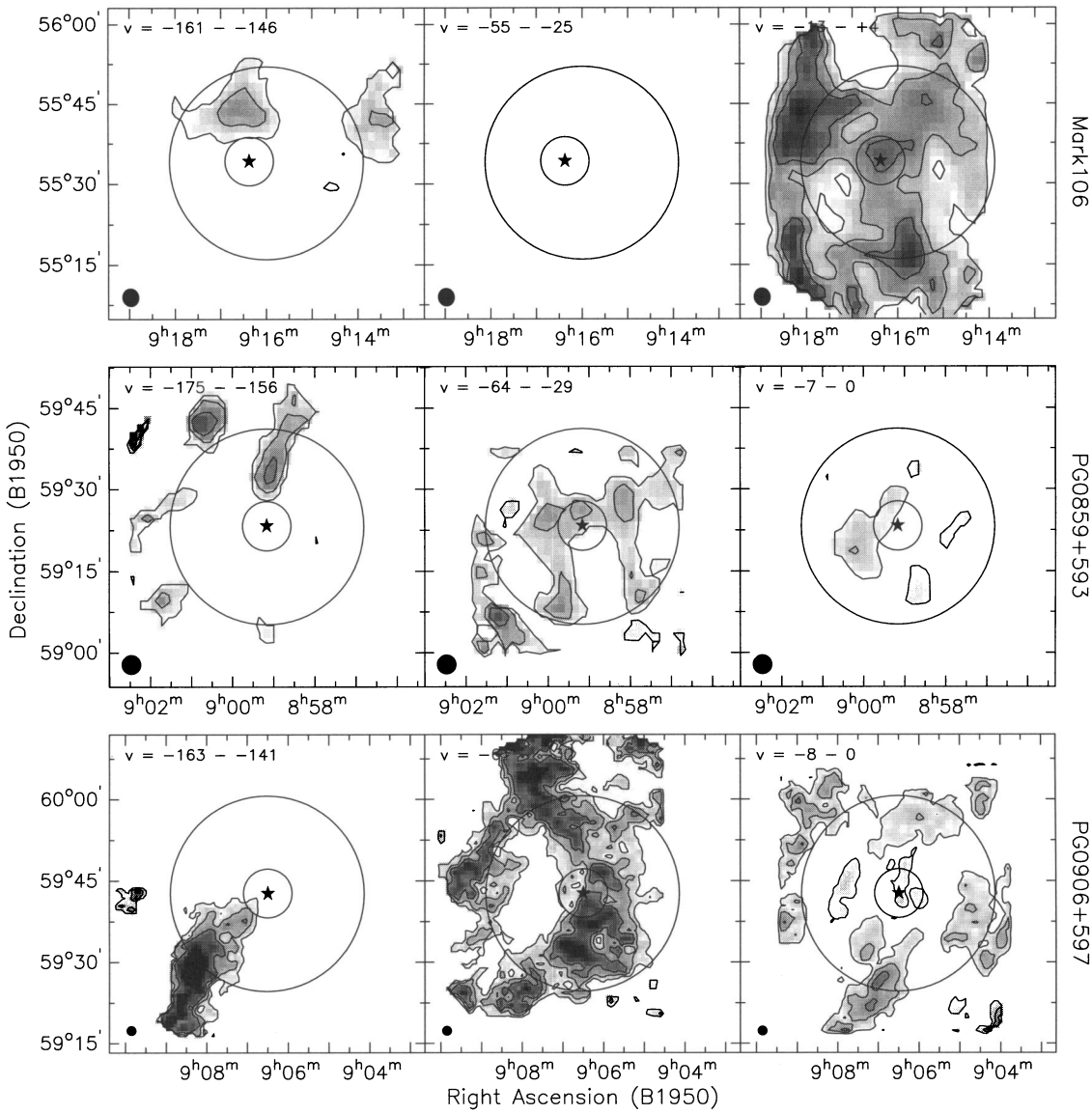


FIG. 3.—Small-scale HVC structure measured at Westerbork around the three probes. The contours of column density are at 0.2, 1, 2, 5, 7.5 and 10 × $10^{19}$ $cm^{-2}$. The Westerbork angular resolution (~2′) is shown by black ellipses in the lower left-hand corners. Asterisks indicate probe positions, and circles show half-power circles for the Effelsberg 100 m dish and the Westerbork 25 m dishes. For each probe, three panels are given, for the high-, intermediate-, and low-velocity gas. The velocity ranges that were summed to get the maps are indicated at the top of the panels.

ference between these two values is the part of the flux that is on scales that are filtered out by the Westerbork beam. To this value must be added the brightness temperature in the direction of the probe that is found at the highest possible resolution [Fig. 4, panel (WSRT)]. A final complication is that structure on scales small enough to be seen by Westerbork can be too faint to detect, which results in an overestimate of the amount of flux on large scales.

To measure the flux recovered within the Effelsberg beams on the probes, the Westerbork maps were smoothed to a beamwidth of 9′ and scaled by 2.08 K $Jy^{-1}$. The resulting profiles toward each of the probes are shown in the panel labeled (WSRT/Eff) in Figure 4. No obvious signal is visible at the velocity of complex A, except at the 0.14 K (4 $\sigma$) level toward PG 0906+597. Elsewhere in the maps, there are concentrations with brightness temperatures of 0.44, 0.36, and 1.06 K for Mrk 106, PG 0859+593, and PG 0906+597, respectively (when smoothed to a 9′ beam). Unfortunately, we do not cover the field fully with Effelsberg beams, and thus we do not know what percentage of the flux would be recovered in those directions.

For the intermediate-velocity clouds in the directions of the probes, the situation is similar to that for the high-velocity clouds. Toward Mrk 106, the IVC is not seen at all in the WSRT maps, but it is also faint (0.41 K) at Effelsberg. Toward the two stars, the IVCs are brighter (1.9 and 5.5 K peak brightness temperatures), and about 20% of the flux within the Effelsberg beams is recovered.

The smallest scale at which structure would get lost in the noise of the Westerbork map can be estimated by means of simulations. Thus, artificial Gaussian sources were constructed, each with a peak brightness temperature of 0.7 K, i.e., approximately the measured value for the HVCs in the Effelsberg beam. For a given fraction $p$ of recovered flux, a fraction $(1 - p)$ of the 0.7 K is on filtered-out scales. The

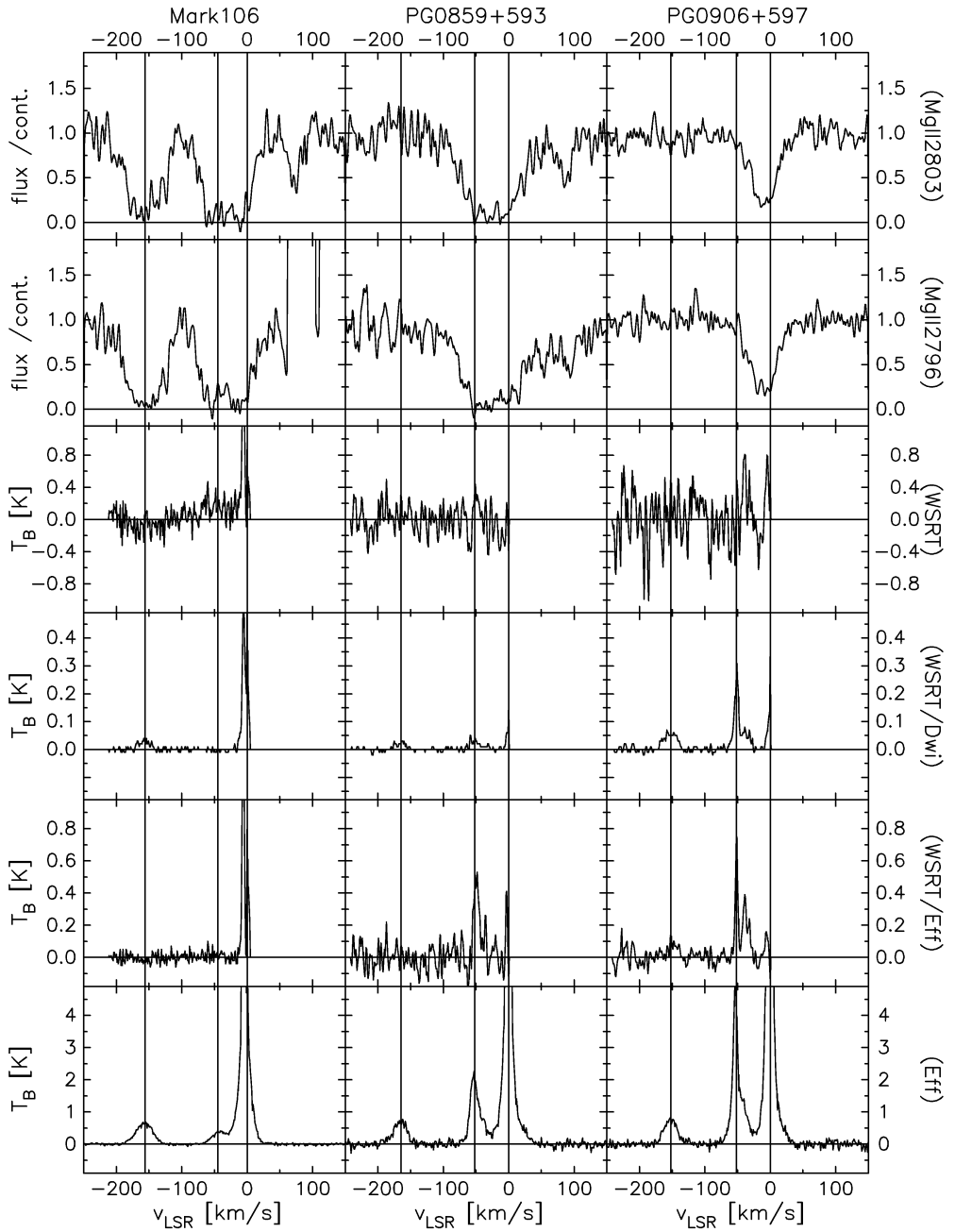


FIG. 4.—H I and Mg II spectra. For each probe, several spectra are given, as specified at the right-hand side of each row of panels. "(Eff)": profiles measured with the Effelsberg 100 m dish at 9′ angular and 1 km $s^{-1}$ velocity resolution. "(WSRT/Eff)": profile measured with the Westerbork telescope, integrated over an equivalent 9′ beam on the probe; the scale is one-fifth of that of the "(Eff)" profile. "(WSRT/Dwi)": profile measured with Westerbork, integrated over the full 36′ beam; the scale is 1/10 of that of the "(Eff)" profile. "(WSRT)": Westerbork profile on the probe, at full resolution. "(Mg II 2796)" and "(Mg II 2803)": *HST* spectra of the probes, normalized by the local continuum.

artificial sources were convolved with the actual dirty beam of the Mrk 106 observation. For a circular source with FWHM 9′, the observed peak would then be 0.52 K. It would be 0.33 K for a source with FWHM 15′ × 15′, 0.15 K for 20′ × 20′, 0.45 K for 9′ × 15′, 0.41 K for 9′ × 20′, and 0 K for a source with FWHM 36′ × 36′. When smoothed to a resolution of 9′, the noise level in the Westerbork maps is 0.04 K. So, assuming a 3 $\sigma$ detection limit, the smallest filtered-out scale is that for which the peak brightness temperature observed with the dirty interferometer beam is less than 0.12 K. This corresponds to structure on scales of about 20′; i.e., any structure in the missing flux that is on smaller scales would have been detected. Thus, this implies that the estimate of the brightness temperature of the filtered-out large-scale structures can be at most 0.12 K too high (3 $\sigma$ limits).

The final brightness temperature estimate toward a probe is given by $T = T_{\rm E} - T_{\rm W,E} + T_{\rm W}$, where $T_{\rm E}$ is the observed $T_B$ at Effelsberg, $T_{\rm W}$ is the observed $T_B$ at the highest resolution at Westerbork, and $T_{\rm W,E}$ is the $T_B$ of the smoothed Westerbork map.

We can give a 1 $\sigma$ confidence level for the final value in the brightness temperature as follows. First, we include the measurement error in the fit to the Effelsberg spectrum

$[\sigma(T_E)]$. Next, we find the minimum possible brightness temperature by subtracting the $\sigma(T_{W,E})$ of smoothed small-scale structure that could have been missed, as explained above. Then we use our experience that the observed structure does not show depressions in a smooth background, but only superimposed bumps, to argue that the contribution of the high-resolution map can only be positive. This implies that the maximum possible brightness temperature is found by adding the error in the high-resolution Westerbork map $[\sigma(T_W)]$. Thus, we find that the brightness temperature toward Mrk 106 must be $0.67^{+0.01}_{-0.01}{}^{+0.14}_{-0.04}$ K, toward PG 0859+593 $0.73^{+0.03}_{-0.03}{}^{+0.17}_{-0.04}$ K and toward PG 0906+597 $0.66^{+0.03}_{-0.03}{}^{+0.30}_{-0.04}$ K. The first term in these errors is the error in the fits to the Effelsberg spectra, while the second term is the systematic error.

To obtain the final column densities, we also take into account the observational fact that the line width of the small-scale structure is about 5–10 km s$^{-1}$ (Cram & Giovanelli 1976; Wakker & Schwarz 1991). Thus, while the actual fitted line width is used to convert the fitting error and downward systematic error to a column density, a line width of 7 km s$^{-1}$ is used to convert the upward systematic error. This yields the final adopted column densities listed in Table 2.

A similar procedure is followed to derive the final column density estimates for the IVCs and LVCs in the fields.

#### 4.3.2. *Flux in the Fine Structure*

To determine what percentage of the flux is in the fine structure detected in the Westerbork maps, the data in each channel were summed and scaled with 0.13 K Jy$^{-1}$, the conversion factor from jansky to Kelvin for the 36′ primary beam of the Westerbork telescope. The resulting spectra are displayed in the panels labeled "(WSRT/Dwi)" of Figure 4. They have a peak $T_B$ of 0.04–0.07 K. Ideally, these values should be compared to a single-dish observation with the Dwingeloo telescope (which has the same beam size) with the beam centered on our probes. However, we do not have such data available, so we can only compare to values interpolated between the grid points of the Hulsbosch & Wakker (1988) survey. This gives 0.75, 0.56, and 0.56 K for Mrk 106, PG 0859+593, and PG 0906+597, respectively. Thus, only about 10% of the flux in the Dwingeloo beams is recovered. This is much less than the values of 25%–50% reported for other fields in complex A (Schwarz & Oort 1981; Wakker & Schwarz 1991). It can be explained by a combination of several effects. First, the current fields have lower brightness temperatures (which was about 3 K for the other fields); thus, any signal is more likely to be below the noise level. Second, the other fields were toward cores of the HVC complex, while the fields discussed here are away from the cores. Apparently, there is less fine structure in those directions.

## 5. *HST* DATA

Seven hours of Cycle 3 *HST* time were allocated for this program. The two stars were observed on 1993 November 7, using side 2 of the GHRS and the G270M grating. Since these observations were made 1 month before the *HST* repair mission, the data suffer from the halo in the point-spread function. The observation for the Seyfert galaxy was deferred to the end of Cycle 4 and was done on 1995 March 13 with the same setup.

The setup employed the STEP-PATT 5 and FP-SPLIT = 4 routines. The former gives four substeps per diode; the latter shifts each subexposure along the diode array to minimize the effect of fixed-pattern noise and bad diodes. The diode spacing was 0.092 Å, or 9.84 km s$^{-1}$. For the stellar spectra the point-spread function has a sharp core with 10 km s$^{-1}$ FWHM, containing about 40% of the light. Superimposed on this are broad wings extending to ±40 km s$^{-1}$. The initial processing of the raw data employed the standard calibration package CALHRS; this procedure is part of the standard Space Telescope Science Institute data pipeline and IRAF reduction packages. The flux calibration includes conversion of raw counts to count rates and corrections for particle radiation contamination, dark counts, known diode nonuniformities, scattered light, paired pulse events, and vignetting. The individual observations are merged into four FP-SPLIT spectra of 2000 points each (four samples per detector diode). Observations of a Pt-Ne lamp, taken immediately prior to the science observations at the same grating carousel position, were used to determine the wavelength scale for the observations. These lamp observations were processed using the standard WAVECAL routine, which creates a lookup table that is used by the CALHRS routine. A conservative error estimate for the absolute assignment of wavelengths is ±one diode or ∼10 km s$^{-1}$. For a detailed review and analysis of the in-orbit performance of the GHRS, see Heap et al. (1995).

The final steps of the reduction process were performed using techniques and software developed and tested at the University of Wisconsin–Madison. The individual FP-SPLIT spectra were aligned and summed. Linear continua are sufficient to fit the regions immediately surrounding the lines of interest. Scattered light removal is allowed for in the GHRS by measuring the light to either side of the order of interest (i.e., in the direction perpendicular to the dispersion); the average of the two off-order measurements is then subtracted from the spectrum. In our spectra, the level of scattered light is low enough that we have not made any additional corrections beyond those made in the raw data calibration. Fixed-pattern noise, arising from imperfections in the photocathode window and from nonuniformities in the photocathode itself, can contribute significantly to the noise level in GHRS data (see Cardelli & Ebbets 1994). In our case, the signal-to-noise ratio of each observation was not sufficient to allow a proper removal of the fixed-pattern noise. However, because we used the FP-SPLIT = 4 option, a simple averaging of spectra shifted along the diode array will reduce the strength of a fixed-pattern noise feature by a factor 4. Therefore, we are confident that our results are not seriously affected. The final spectra are shown in Figure 4.

Low-velocity Mg II absorption is clearly visible in all three spectra. In the spectra of the two stars, this line does not have the sharp edges expected for a saturated line, but the line shape can be understood as a result of the degraded pre-COSTAR point-spread function. At first sight, it is worrisome that the counts do not go down to zero. However, the stars are very faint so that the total number of counts is very low. The offset thus is within the error in the determination of the subtracted dark count. The latter is 0.011 counts s$^{-1}$ per diode, which corresponds to about 30 counts per diode for the two star exposures (3279 and 2767 s) and 75 counts per diode for Mrk 106 (6960 s). This gives an error in the subtraction of the background count of order 5 and 8

counts, respectively. The total number of counts in the continuum is between 30 and 80, so that the error in the relative flux due to the background subtraction is about 6%–20%.

The absorption lines were fitted to estimate equivalent widths and lower limits to the $Mg^+$ column density. The results are given in Table 2. The Mg II absorption due to the low- and intermediate-velocity gas overlaps. We assigned absorption at $v_{LSR} < -30$ or $-25$ km s$^{-1}$ (for Mrk 106 or PG 0859+593) to the intermediate-velocity clouds and absorption at $v > -30$ or $-25$ km s$^{-1}$ to the low-velocity cloud. These are the velocities at which the H I spectrum shows a minimum. In the table, errors for detected lines are 1 $\sigma$ errors, while detection limits are 3 $\sigma$ limits.

The spectrum of Mrk 106 suffers from the presence of a bad diode, which gives rise to four spikes in the $\lambda$2796 spectrum (one for each substep), at velocities above +50 km s$^{-1}$.

We will discuss the $Mg^+$ absorption in the next section. Here we note the presence of a dip at a velocity of about +80 km s$^{-1}$ in the spectrum of PG 0859+593 and the $\lambda$2803 component of Mrk 106. We are unable to identify this "absorption." It is unlikely to be instrumental as it is not seen toward PG 0906+597. The line ratio in the PG 0859+593 spectrum is the opposite of what is expected if it were an Mg II line, and no H I counterpart is seen. If this absorption had been seen only toward PG 0859+593, it might have been possible to argue that it was a saturated stellar absorption seen over only part of the stellar surface. But that would leave the line toward Mrk 106 unexplained.

## 6. DERIVATION OF DISTANCE LIMITS

High-velocity Mg II absorption is clearly seen in the spectrum of Mrk 106. The line is strongly saturated, with an equivalent width of 490 $\pm$ 26 mÅ ($\lambda$2803 component). This implies a column density $\gg 5 \times 10^{13}$ cm$^{-2}$ and an abundance $A = N(\text{Mg II})/N(\text{H I}) \gg 1.3 \times 10^{-6}$ for Mg II. The standard solar abundance of Mg is $3.8 \times 10^{-4}$ (Anders & Grevesse 1989), while in low-velocity gas, the abundance of $Mg^+$ is typically $4.8 \times 10^{-6}$ (Jenkins 1987).

High-velocity absorption is not detected toward the two stars. To derive an upper limit to the equivalent width, we use the errors that would result from fitting a Gaussian to the line profile:

$$\sigma(W) = \frac{\lambda}{c}\sqrt{3\sqrt{\frac{\pi}{8\ln 2}}}\frac{\sqrt{h\gamma}}{(\text{S/N})_c}$$

(Kaper et al. 1966). Here $h$ is the grid spacing (9.84 km s$^{-1}$); $\gamma$ is the estimated FWHM of the line, which we set to 10 km s$^{-1}$, i.e., a line that would have an FWHM of one resolution element; $(\text{S/N})_c$ is the signal-to-noise ratio in the continuum. This yields 1 $\sigma$ detection limits of $144/(\text{S/N})_c$ mÅ, or 32 and 16 mÅ for PG 0859+593 and PG 0906+597, respectively. Using the H I column densities, these limits correspond to 3 $\sigma$ upper limits to the $Mg^+$ abundance in front of the stars of $6.8 \times 10^{-8}$ and $4.1 \times 10^{-8}$. These upper limits are obviously much less than the lower limit $\gg 130 \times 10^{-8}$ found toward Mrk 106. *Thus, we can confidently conclude that the northern part of complex A is behind both stars. This implies that complex A must be more distant than 4 kpc and that its z-height must be more than 2.5 kpc.*

For the mass of complex A, the distance limit implies $M > 1.5 \times 10^5$ $M_\odot$. The linear size (5° × 35°) must be $> 0.3 \times 2.5$ kpc. The total kinetic energy is more difficult to estimate, as we do not know the cloud's tangential velocity. It is reasonable to use the average deviation velocity as a minimum estimate of the peculiar velocity of the HVC. This is 125 km s$^{-1}$ (Wakker & van Woerden 1991), which corresponds to a kinetic energy of $> 2.5 \times 10^{45}$ J, equivalent to $>25$ supernovae.

The intermediate-velocity cloud at velocities around $-50$ km s$^{-1}$ can be identified as the "Low-Latitude Intermediate-Velocity Arch," or LLIV Arch (Kuntz & Danly 1996). From the nondetection in the spectrum of SA 12 391 (observed by Lilienthal et al. 1990), Kuntz & Danly (1996) derived a lower limit to its $z$-height of 1.1 kpc ($d > 1.7$ kpc). SA 12 391 is very close to our two stars (see Fig. 1). Toward PG 0906+597, the LLIV Arch is not detected in absorption, either (abundance $< 1.1 \times 10^{-8}$). Since it is clearly detected toward Mrk 106 (abundance $\gg 160 \times 10^{-8}$) and PG 0859+593 (abundance $\gg 75 \times 10^{-8}$), we can conclude that the LLIV Arch is between our two stars, as well as more distant than SA 12.391, i.e., $1.7 < d < 4$ kpc, or $1.1 < z < 3$ kpc. The LLIV Arch was also detected in the spectrum of PG 0832+675 (Schwarz et al. 1995). The distance to this star is uncertain, however (see § 2.3). Both estimates of its distance (31 and 2.5 kpc) are consistent with the detection of the LLIV Arch in its spectrum. The lower estimate would constrain the distance of the IVC to $1.7 < d < 2.5$ kpc.

## 7. DISCUSSION

With a firm lower distance limit in hand for HVC complex A and with a distance bracket now known for the LLIV Arch, we can judge many of the models previously proposed for HVCs and IVCs. The list of possible explanations for HVCs given by Oort (1966) still remains the most useful basis for this. Van Woerden, Schwarz, & Hulbosch (1985) rediscussed most of the explanations for HVCs, while Wakker (1991a) extended Oort's list with later suggestions. Kuntz & Danly (1996) give a summary of the interpretations for the northern IVCs, of which the LLIV Arch is one. They found a distance bracket of $1 < z < 2$ kpc for the larger Intermediate-Velocity Arch and suggested that the LLIV Arch is a similar structure but somewhat more distant. Our distance bracket supports this conclusion.

Many of the proposed origins for IVCs are the same as those for HVCs. We will shortly revisit the possible interpretations, as applicable to complex A and the LLIV Arch, sorted in terms of ascending distance at which the complex is placed. More thorough discussions can be found in the aforementioned papers and in the papers referenced below.

1. *Complex A is a ghost of nearby molecular clouds.* Verschuur (1990) suggested that for several HVCs, most notably complex A, the contours of nearby CO clouds reflects the fine structure. He concluded that the HVCs are at distances similar to those of the CO clouds, taken to be between 200 and 800 pc. This model clearly is inconsistent with our results, and it can be put aside.

2. *Complex A and/or the LLIV Arch are part of a nearby supernova shell.* Oort (1966) considered this as one of the first suggestions to explain HVCs, at a time when only complex A and part of complex C were known. His original argument to reject this model was that the mass of such a supernova shell would be at least $10^3$ $M_\odot$ (for an assumed distance of 300 pc). Our distance limit/bracket would increase this to $M > 2 \times 10^5$ and $> 5 \times 10^4$ $M_\odot$ for the HVC and IVC, respectively. These are too high to be pro-

duced by a single supernova, and the presence of many correlated supernovae at high $z$ is unlikely. Further, in order to see the shell, it would have to expand through a low-density medium, a condition not supported by observations for the local ISM. This model is now definitively excluded for complex A, as well as for the IV and LLIV Arches (see also Kuntz & Danly 1996).

3. *Complex A is a nearby result of a collision of an* H I *cloud with the disk.* Meyerdierks (1991, 1992) proposed that the H I data for the high-, intermediate-, and low-velocity gas in the region around the lowest latitude core of complex A (A 0), were consistent with the idea that a high-velocity neutral hydrogen bullet fell into the Galactic disk at an oblique angle, with a velocity of 325 km $s^{-1}$. Since the IVC in this region is part of the North Celestial Pole loop of IVCs, a distance of order 250 pc is implied by Meyerdierks's model. Our distance limit is for a different part of complex A, some 30° away from A 0. However, if one makes the reasonable assumption that the complex is a single structure, Meyerdierks's model can be saved only if complex A points straight at the Sun and is about 16 pc wide at its tip, but at least 1 kpc wide at the high-latitude end. This is a very unlikely geometry, so we conclude that the signs of interaction that Meyerdierks saw were not genuine.

4. *Complex A and/or the LLIV Arch are part of a supernova explosion in the Perseus arm.* Rickard (1968) analyzed H I and optical data of the region $\ell = 90°$–$150°$, $b \simeq 0$, $v_{LSR} = -100$ to $+20$ km $s^{-1}$ and found that he could best explain the velocities in the plane by a supershell expanding at 20–30 km $s^{-1}$ with its center toward $\ell = 120°$, up to 100 pc above the plane, at a distance of 3 kpc. He suggested that this was the result of the cumulative effect of many supernovae. He further suggested that the northern HVC complexes A and C might be lower density clumps ejected to large $z$-heights. This would imply a distance of order 1 kpc for complex A. Verschuur (1993) constructed an elaborate model for the velocity and space distribution of a supershell originating in the Perseus arm, in which he tried to explain both the large northern HVCs and the northern IVCs in a unified way. Distances for HVC complexes A and C of a few hundred parsecs are then suggested. Both these models are incompatible with the strong lower distance limit that we derive. The IVCs are included in this model, but the available data did not allow a comparison of the predictions with observations. Kuntz & Danly (1996) present the necessary data and point out that the model predicts an increase in velocity with lower $z$, which is the opposite of the pattern seen in the IV arch. The LLIV Arch is at constant Galactic latitude, so we cannot properly judge this prediction for it. The supershell models correspond to what Wakker & Bregman (1991) term the "cannonball" model, in which high-velocity gas is ejected from the disk in the form of neutral clouds. The resulting sky and velocity distributions are inconsistent with the observations when the whole sky is considered. We conclude that an explanation in which complex A is part of a supershell is no longer viable but that it can not be excluded for the LLIV Arch.

5. *Complex A and/or the LLIV Arch are partly primordial intergalactic gas being accreted by the Galaxy while sweeping up high-z neutral hydrogen.* This hypothesis was one of Oort's (1966) original suggestions for the HVCs, but it could also be applicable to IVCs. It is similar to the model proposed by Meyerdierks (discussed above), except that the implied distance is on the order of 1 kpc. Oort (1970) elaborated on this model and suggested that there is gas left over from the formation of the Galaxy that is only now reaching the disk. As it approaches the disk, it sweeps up high-$z$ (1–2 kpc) cold, low-density coronal gas, is shock heated, and cools again. About 70% of the HVC would consist of swept-up gas, the rest being primordial. The high velocities are due to an outside overpressure provided by the infalling cloud. The signature of an interaction of an infalling sheet was calculated from hydrodynamic models by Tenorio-Tagle (1981) and Tenorio-Tagle et al. (1986). They find that single-sided shells could be produced, which explains the fact that only negative velocities are seen. Two problems with this picture were identified by Oort (1970): could coherent gas clouds survive for $\sim$10 Gyr before impacting the Galaxy, and would the gas cool quickly enough after being shocked so that it would be visible at $z$-distances of order 1 kpc?

Oort & Hulsbosch (1978) and Hulsbosch (1979) used the velocity and angular structure data then available for complex A to make this their favorite model. They argued that the erratic velocity jumps observed by Giovanelli et al. (1973) imply a cloud that is less than 10 Myr old and that these are the consequence of collisions with halo gas. The steep edges observed (at 10′ resolution) would be shock fronts. However, the Westerbork data of Wakker & Schwarz (1991) show that the steep edges break up into a random collection of clumps at higher resolution. A similar study does not exist for IVCs. However, our Westerbork data (Fig. 3) for the IVCs in our fields suggest that the same breakup phenomenon may also occur.

This model requires the presence of cold low-velocity gas at high $z$. Our distance limit implies that this model can be retained for complex A only if such gas exists in sufficient quantities at $z$-heights of at least 2.5 kpc. It is not clear whether or not that is compatible with observations. Even the so-called Lockman layer of high-$z$ neutral hydrogen (Lockman & Gehman 1991) does not reach much farther out than 1 kpc.

6. *Complex A is part of a galactic fountain.* The idea that has gained the most ground as an explanation of the HVCs and IVCs in general, and complex A in particular, has been that of the galactic fountain. It was first put forward by Shapiro & Field (1976). In the fountain model, hot gas is produced by the cumulative effect of supernovae in the disk. Thermal expansion makes it rise to large $z$-heights, where it becomes unstable; cool clouds condense and fall back to the disk ballistically. In effect, this sets up a galactic-scale convection. A similar suggestion was made by Suchkov & Schchekinov (1974) and Schchekinov (1977), who instead suggested spiral shocks as the heating mechanism. Oort (1966) discussed a model in which the clouds form at similar $z$-heights, but he did not indicate a mechanism to generate the hot gas. The difference with the previous model is that the clouds would form in the Galactic halo, instead of being primordial objects currently reaching the Galaxy. Also, the angular and velocity structure can be set up at formation, instead of at the time when the cloud starts interacting with the lower $z$ gas.

The fountain model was first suggested as a possible explanation for the HVCs by Bregman (1980). Further work by Kahn (1990), Houck & Bregman (1990), and Li & Ikeuchi (1992) showed that the energy input from supernovae may be sufficient to set up a fountain, although the maximum predicted vertical velocity is only of the order of 70–100 km $s^{-1}$, far less than the observed LSR velocities of

many HVCs. Wakker (1991b) showed that accounting for projection effects due to galactic rotation can reconcile the observed velocities with the fountain model. Most HVCs would lie at galactocentric distances between 10 and 20 kpc and $z$-heights of 0–10 kpc. A possible problem may be that the feeding of hot gas to the halo by means of superbubble breakout might be prevented by magnetic fields (Tomisaka 1990, 1992).

If we combine the typical observed column density ($10^{20}$ cm$^{-2}$), diameter (2°), and velocity dispersion of the envelopes (25 km s$^{-1}$) of the clouds with a distance limit of 4 kpc, the implied volume density is $n < 0.25$ cm$^{-3}$, and the pressure would be $P < 3500$ cm$^{-3}$ K. Such a cold neutral cloud would be in pressure equilibrium with a hot ($10^6$ K) corona if the latter has a density of $<0.0035$ cm$^{-3}$. From a similar calculation, but assuming $d = 1$ kpc, Oort (1966) derived $n = 0.025$ cm$^{-3}$ for the hot corona. For an LLIV Arch core, the typical column density is more like $3 \times 10^{19}$ cm$^{-2}$, while the size and velocity width are similar. Thus, at a distance of 3 kpc, the density is 0.33 cm$^{-3}$. A $10^6$ K halo would have to have a density of 0.0045 cm$^{-3}$ at $z = 2.5$ kpc to be in equilibrium.

These density estimates can be compared with the data of Snowden, MacCammon, & Verter (1993), who used *ROSAT* observations of the foreground emission in the direction of a nearby molecular cloud to derive a density of 0.006 cm$^{-3}$ and a pressure of 12,500 cm$^{-3}$ K in the plane for the $10^6$ K gas. So, while Oort (1966) concluded that the observations of complex A were incompatible with the assumption of pressure equilibrium with a hot halo, our lower limit to the distance shows that such pressure equilibrium can exist if the halo has a scale height of several ($>3$) kpc. There is some observational evidence for this, based on C IV absorption lines of high-$z$ halo stars (Sembach & Savage 1992) and *ROSAT* shadowing data (Herbstmeier et al. 1995).

7. *Complex A and/or the LLIV Arch is a high-z spiral arm.* Davies (1972a, 1972b, and 1974) and Verschuur (1973a, 1973b, 1975) advocated a model in which the lower latitude HVCs ($b < 30°$) are part of an extreme warp of the Galaxy, with galactocentric distances of order 20 kpc, centered on $\ell = 130°$. The HVCs would then be a disconnected continuation of the Outer Arm (Habing 1966; Kepner 1970) but would still be part of the spiral pattern. For the HVCs this model is unlikely because of problems with the implied geometry, morphology, and velocities (Hulsbosch & Oort 1973). Our distance bracket for the LLIV Arch places it above the Perseus Arm, which suggests that this model may be applicable. If this were so, then there would not be a unified explanation for the HVCs and IVCs.

Several models for complex A place it at large distances from the Sun. All of these are compatible with our lower distance limit, although other arguments pro or con may exist. To complete our inventory, we briefly summarize them.

8. *Complex A was ejected from the Galactic nucleus.* If between 80 and 150 Myr ago our Galaxy was a Seyfert galaxy, the Galactic center might have ejected large amounts of gas, which are only now falling back toward the disk (Oort 1966; Kundt 1987). There is little supporting evidence for this model, especially since a very low angular momentum is predicted and the velocities have to be fine tuned to get the current situation.

9. *Complex A is part of a polar ring around the Galaxy.* Haud (1988) suggested that the Magellanic Stream and HVC complex C form part of a polar ring of neutral hydrogen around our Galaxy, at a distance of 90 kpc. Complex A is problematic in this model as it is not in the ring.

10. *Complex A was drawn out of the Magellanic Clouds during a previous passage.* This model was rejected by Oort & Hulsbosch (1978) because it implies the gas stays together for about 1 Gyr, which appears incompatible with the internal velocity differences unless the confining hot gas in the Galactic halo reaches out to 50 kpc from the disk. Wakker & Bregman (1990) also found that with any realistic orbit of the Magellanic Clouds it was not possible to obtain gas at the observed negative velocities in the sky quadrant of complex A.

11. *Complex A is a satellite of the Galaxy or connected to globular clusters and nearby dwarf galaxies.* This possibility was included in Oort's (1966) list. The option that complex A is an independent satellite of the Galaxy was advocated by Kerr & Sullivan (1969), while a connection with globular clusters was favored by Lynden-Bell (1976). The model implies a very large distance ($>20$ kpc) and size ($>1 \times 10$ kpc) but a very low volume density ($<0.05$ cm$^{-3}$). Some support was lent by Dyson & Hartquist (1983), who showed that star formation can maintain the observed turbulent velocity dispersion if the cloud consists of a collection of cloudlets moving at random velocities. The level of star formation could be low enough that few O and B stars are produced. PG 0832+675 could be one of these stars if it is a main-sequence star. In this model, the observed Ca and Mg are produced by past star formation. It further predicts an overabundance of old cool stars in the direction of the HVC. This model might explain complex A, but it cannot account for the velocity and sky distribution of all HVCs (Wakker 1991b).

## 8. CONCLUSION

We derive a strong lower limit of 4 kpc ($z > 2.5$ kpc) to the distance of HVC complex A. This allows us to exclude confidently several of the proposed models that put this HVC close to the Sun and close to the Galactic plane. This does not necessarily exclude such models for all HVCs, unless one assumes that they are all part of the same phenomenon, rather than allowing separate explanations for individual HVCs.

For the LLIV Arch we derive a distance bracket $1.7 < d < 4$ kpc ($1.1 < z < 3$ kpc), which approximately places it above the Perseus arm. This distance is compatible with the suggestion of Kuntz & Danly (1996) that the LLIV Arch is similar to the IV Arch, but somewhat more distant.

We can exclude that complex A is a ghost of nearby molecular clouds. We can also exclude that complex A and/or the LLIV Arch are a nearby supernova shell or fragments of a superexplosion in the Perseus arm that are now close to the Sun. We can further exclude an interaction with low-$z$ disk gas, although we can not exclude an interaction with a high-$z$ extension of the gaseous disk.

From our distance limit and distance bracket, we derive that the internal structure and volume density are compatible with an interpretation in which complex A and the LLIV Arch are several kiloparsecs above the plane, embedded in a hot gaseous halo. This conclusion is independent of whether or not they formed in the manner proposed in the fountain model. A model in which the clouds consist of primordial gas accreting onto the Galaxy could be saved if

the presence of cool high-$z$ gas can be proved or if a different way can be found to set up the angular and velocity structure. Differentiation between these two models would be possible if we knew the intrinsic metallicity. The fountain model predicts near-solar metallicity; the accretion model predicts about 70% of that.

For the LLIV Arch, our distance bracket is compatible with the idea that it is a high-$z$ spiral arm. In that case, its origin may be different from that of HVCs.

Our distance limit does not exclude any of the interpretations that place complex A more than 10 kpc from the Sun, although these are less likely when secondary arguments based on the sky and velocity distribution of HVCs are taken into consideration.

The detection of an Mg II absorption in the spectrum of the Seyfert galaxy Mrk 106 provides additional evidence that HVCs are not made out of primordial material. The advantages and disadvantages of using the Mg II lines for this work are clearly shown. The advantage is that very small amounts of Mg II will produce saturated absorption, so that the interpretation of nondetections becomes more clear-cut. The disadvantage of the Mg II lines is that we cannot derive the $Mg^+$ abundance, and thus we cannot distinguish between models that predict different metallicities for the HVCs.

In order to make further progress on the question of the distance to HVCs, we need to find additional stellar probes (ideally BHB stars) both in front and behind complex A. A directed search for such probes will be necessary.

Support for this work was provided by NASA through grant GO-04536.01-92A to B. W. from the Space Telescope Science Institute, which is operated by the Association of Universities for Research in Astronomy, Inc., under NASA contract NAS5-26555.

T. C. B. acknowledges partial support provided by the National Science Foundation in the form of grants AST 90-1376 and AST 92-22326. R. W. acknowledges partial support from the teaching postdoctoral program in the Department of Physics and Astronomy at Michigan State University.

The Westerbork Radio Observatory is operated by the Netherlands Foundation for Research in Astronomy (ASTRON/NFRA) with financial support from NWO.

The Effelsberg Telescope belongs to the Max Planck Institut für Radio Astronomie at Bonn.

We thank Arthur Coolen of ASTRON for help with the calibration of the Westerbork observations and Peter Kalberla of the University of Bonn for doing the Effelsberg observations. The authors would like to extend thanks to A. Sarajedini and B. Anthony-Twarog for obtaining photometric measurements and performing data reduction for the stellar probes discussed in this paper. Finally, the authors would also like to thank U. Heber for carrying out a preliminary spectral analysis of PG 0906+597 and for comments on possible interpretations of this interesting star.

## REFERENCES

Anders, N., & Grevesse, E. 1989, Geochim. Cosmochim. Acta, 53, 197
Bajaja, E., Cappa de Nicolau, C. E., Cersosimo, J. C., Martin, M. C., Loiseau, N., Morras, R., Olano, C. A., & Pöppel, W. G. L. 1985, ApJS, 58, 143
Beers, T. C., Doinidis, S. P., Griffin, K. E., Preston, G. W., & Shectman, S. A. 1992, AJ, 103, 267
Beers, T. C., Preston, G. W., & Shectman, S. A. 1988, ApJS, 67, 461
Beers, T. C., Wilhelm, R. J., Doinidis, S. P., & Mattson, C. 1996, ApJS, 103, 433
Bregman, J. N. 1980, ApJ, 236, 577
Brown, P. J. F., Dufton, P. L., Keenan, F. P., Boksenberg, A., King, D. L., & Pettini, M. 1989, ApJ, 339, 397
Burstein, D., & Heiles, C. 1982, AJ, 87, 1165
Cardelli, J. A., & Ebbets, D. C. 1994, in Calibrating the Hubble Space Telescope, ed. J. C. Blades & S. J. Osmer (Baltimore: Space Telescope Science Institute), 322
Cram, T. R., & Giovanelli, R. 1976, A&A, 48, 39
Crawford, D. L. 1975, PASP, 87, 481
Danly, L. 1989, ApJ, 342, 785
Danly, L., Albert, C. E., & Kuntz, K. D. 1993, ApJ, 416, L29
Davies, R. D. 1972a, MNRAS, 160, 381
———. 1972b, Nature, 237, 88
———. 1974, in IAU Symp. 60, Galactic Radio Astronomy, ed. F. J. Kerr & S. C. Simonson III (Dordrecht: Reidel), 599
Davies, R. D., Buhl, D., & Jafalla, J. 1976, A&AS, 23, 181
de Boer, K., Altan, A., Bomans, D., Lilienthal, D., Moehler, S., van Woerden, H., Wakker, B., & Bregman, J. 1994, A&A, 286, 925
Dreizler, S., Heber, U., Werner, K., Moehler, S., & de Boer, K. S. 1990, A&A, 235, 234
Drilling, J. S., & Beers, T. C. 1995, ApJ, 446, L27
Dyson, J. E., & Hartquist, T. W. 1983, MNRAS, 203, 1233
Giovanelli, R. 1980, AJ, 85, 1155
Giovanelli, R., & Haynes, M. P. 1977, A&A, 54, 909
Giovanelli, R., Verschuur, G. L., & Cram, T. R. 1973, A&AS, 12, 209
Green, R. F. 1980, ApJ, 238, 685
Green, R. F., Schmidt, M., & Liebert, J. 1986, ApJS, 61, 305
Habing, H. J. 1966, Bull. Astron. Inst. Netherlands, 18, 323
Hambly, N. C., Dufton, P. L., Keenan, F. P., & Lumsden, S. L. 1996, MNRAS, 278, 811
Haud, U. 1988, A&A, 198, 125
Heber, U., Dreizler, S., & Hagen, H.-J. 1996, A&A, in press
Herbstmeier, U., Mebold, U., Snowden, S. L., Hartmann, D., Burton, W. B., Moritz, P., Kalberla, P. M. W., & Egger, R. 1995, A&A, 298, 606
Heap, S. R., et al. 1995, PASP, 107, 871
Houck, J. C., & Bregman, J. N. 1990, ApJ, 352, 506
Hulsbosch, A. N. M. 1968, Bull. Astron. Inst. Netherlands, 20, 33
———. 1978, A&AS, 33, 383
———. 1979, in IAU Symp. 84, The Large Scale Characteristics of the Galaxy, ed. W. B. Burton (Dordrecht: Reidel), 525
Hulsbosch, A. N. M., & Oort, J. H. 1973, A&A, 22, 153
Hulsbosch, A. N. M., & Raimond, E. 1966, Bull. Astron. Inst. Netherlands, 18, 413
Hulsbosch A. N. M., & Wakker, B. P. 1988, A&AS, 75, 191
Jenkins, E. B. 1987, in Interstellar Processes, ed. D. J. Hollenbach & H. A. Thronson, Jr. (Dordrecht: Reidel), 533
Kaelble, A., de Boer, K. S., & Grewing, M. 1985, A&A, 143, 408
Kahn, F. D. 1990, in IAU Colloq. 120, Structure and Dynamics of the Interstellar Medium, ed. G. Tenorio-Tagle, M. Moles, & J. Melnick (Berlin: Springer), 474
Kalberla, P. M. W., Mebold, U., & Reich, W. 1980, A&A, 82, 275
Kalberla, P. M. W., Mebold, U., & Reif, K. 1982, A&A, 106, 190
Kaper, H. G., Smits, D. W., Schwarz, U. J., Takakubo, K., & van Woerden H. 1966, Bull. Astron. Inst. Netherlands, 18, 465
Keenan, F. P., Shaw, C. R., Bates, B., Dufton, P. L., & Kemp, S. N. 1995, MNRAS, 272, 599
Kepner, M. E. 1968, Bull. Astron. Inst. Netherlands, 20, 98
———. 1970, A&A, 5, 444
Kerr, F. J., & Sullivan, W. T., III. 1969, ApJ, 158, 115
Kundt, W. 1987, Ap&SS, 129, 195
Kuntz, K. D., & Danly, L. 1996, ApJ, 457, 703
Li, F., & Ikeuchi, S. 1992, ApJ, 390, 405
Lilienthal, D., Meyerdierks, H., & de Boer, K. S. 1990, A&A, 240, 487
Lockman, F. J., & Gehman, C. S. 1991, ApJ, 382, 182
Lu, L., Savage, B. D., & Sembach, K. R. 1994, ApJ, 426, 563
Lynden-Bell, D. 1976, MNRAS, 174, 695
Massey, P., Strobel, K., Barnes, J. V., & Anderson, E. 1988, ApJ, 328, 315
Meyerdierks, H. 1991, A&A, 251, 269
———. 1992, A&A, 253, 515
Moehler, S., Heber, U., & de Boer, K. S. 1990a, A&A, 239, 265
Moehler, S., Richtler, T., de Boer, K. S., Dettmar, R.-J., & Heber, U. 1990b, A&AS, 86. 53
Muller, C. A., Oort, J. H., & Raimond, E. 1963, CR Acad. Sci. Paris, 257, 1661
Murphy, E. M., Lockman, F. J., & Savage, B. D. 1995, ApJ, 447, 642
Oort, J. H. 1966, Bull. Astron. Inst. Netherlands, 18, 421
———. 1970, A&A, 7, 381
Oort, J. H., & Hulsbosch, A. N. M. 1978, in Astronomical Papers Dedicated to B. Strömgren, ed. A. Reiz & T. Anderson (Copenhagen: Copenhagen Univ. Observatory), 78
Preston, G. W., Shectman, S. A., & Beers, T. C. 1991, ApJ, 375, 121

Rickard, J. J. 1968, ApJ, 152, 1019
Robertson, J. G. H., Schwarz, U. J., van Woerden, H., Murray, J. D., Morton, D. C., & Hulsbosch, A. N. M. 1991, MNRAS, 248, 508
Sasselov, D. D., ed. 1993, ASP Conf. Ser. 45, Luminous High-Latitude Stars (San Francisco: ASP)
Schchekinov, Yu. A. 1977, Astrophysics, 134, 711
Schwarz, U. J., & Oort, J. H. 1981, A&A, 101, 305
Schwarz, U. J., Sullivan, W. T., III, & Hulsbosch, A. N. M. 1976, A&A, 52, 133
Schwarz, U. J., Wakker, B. P., & van Woerden, H. 1995, A&A, 302, 364
Sembach, K. R., & Savage, B. D. 1992, ApJS, 83, 147
Shapiro, P. R., & Field, G. B. 1976, ApJ, 205, 762
Snowden, S. L., MacCammon, D., & Verter, F. 1993, ApJ, 409, L21
Songaila, A., Cowie, L. L., & Weaver, H. F. 1988, ApJ, 329, 580
Suchkov, A. A., & Schchekinov, Yu. A. 1974, Astrophysics, 10, 2
Tenorio-Tagle, G. 1981, A&A, 94, 338
Tenorio-Tagle, G., Bodenheimer, P., Różyczka, M., & Franco, J. 1986, A&A, 170, 107
Theissen, A., Moehler, S., Heber, U., & De Boer, K. S. 1993, A&A, 273, 524
Thejll, P., Bauer, F., Saffer, R., Liebert, J., Dunze, D., & Shipman, H. L. 1994, ApJ, 433, 819
Tomisaka, T. 1990, ApJ, 361, L5
———. 1992, PASJ, 44, 177
Twarog, B. A., & Anthony-Twarog, B. J. 1995, AJ, 109, 2828
van Woerden, H., Schwarz, U. J., & Hulsbosch, A. N. M. 1985, in IAU Symp. 106, The Milky Way Galaxy, ed. H. van Woerden, R. J. Allen, & W. B. Burton (Dordrecht: Reidel), 387
van Woerden, H., Schwarz, U. J., Wakker, B. P., & Peletier, R. F. 1996, in preparation
Véron-Cetty, M.P., & Véron, P. 1995, A Catalogue of Quasars and Active Nuclei (ESO Sci. Rept. 17) (7th ed.; Garching: ESO)
Verschuur, G. L. 1973a, A&A, 22, 139
———. 1973b, A&A, 27, 407
———. 1975, ARA&A, 13, 257
———. 1990, ApJ, 361, 497
———. 1993, ApJ, 409, 205
Wakker, B. P. 1991a, in IAU Symp. 144, The Interstellar Disk-Halo Connection in Galaxies, ed. H. Bloemen (Dordrecht: Kluwer), 27
———. 1991b, A&A, 250, 499
———. 1991c, A&AS, 90, 495
Wakker, B. P., & Boulanger, F. 1986, A&A, 170, 84
Wakker, B. P., & Bregman, J. N. 1990, in Interstellar Neutral Hydrogen at High-Velocities, Ph.D. thesis, B. P. Wakker, chap. 5., Rijks Universiteit Groningen
Wakker B. P., & Schwarz, U. G. 1988, A&A, 200, 312
———. 1991, A&A, 250, 484
Wakker, B. P., & van Woerden, H. 1991, A&A, 250, 509
Wakker, B. P., van Woerden, H., Schwarz, U. J., Peletier, R. F., & Douglas, N. G. 1996, A&A, 306, L25
Wilhelm, R. 1995, Ph.D. thesis, Michigan State Univ.